https://doi.org/10.5194/angeo-2021-39
Preprint. Discussion started: 20 July 2021

Annales Geophysicae Discussions

Modelling of the influence of meteoric smoke particles on artificial heating in the D-region

Margaretha Myrvang[1], Carsten Baumann[2], and Ingrid Mann[1]

[1]UiT The Arctic University of Norway, Department of Physics and Technology, Postboks 6050 Langnes, 9037 Tromsø
[2]German Aerospace Center, Institute for solar-Terrestrial Physics, 17235 Neustrelitz, Germany

Correspondence: Margaretha Myrvang (margaretha.myrvang@uit.no)

Abstract. We investigate if the presence of meteoric smoke particles (MSP) influences the electron temperature during artfical heating in the D-region. The presence of MSP can result in height regions with reduced electron density, so-called electron bite-outs, due to charging of MSP by electrons. Artificial heating depends on the height variation of electron density. By transferring the energy of powerful high frequency radio waves into thermal energy of electrons, artificial heating increases the electron temperature. We simulate the influence of the artificial heating by calculating the intensity of the upward propagating radio wave. The electron temperature at each height is derived from the balance of radio wave absorption and cooling through elastic and inelastic collisions with neutral species.

The influence of MSP is investigated by including results from a one-dimensional height-dependent ionospheric model that includes electrons, positively and negatively charged ions, neutral MSP, singly positively and singly negatively charged MSP and photo chemistry such as photo ionization and photo detachment. We apply typical ionospheric conditions and find that MSP can influence both the magnitude and the height profile of the heated electron temperature above 80 km, however this depends on ionospheric conditions. During night, the presence of MSP leads to more efficient heating, and thus a higher electron temperature, above altitudes of 80 km. We found differences up to 1000 K in temperature for calculations with and without MSP. When MSP are present, the heated electron temperature decreases more slowly. The presence of MSP does not much affect the heating below 80 km for night conditions. For day conditions, the difference between the heated electron temperature with MSP and without MSP is less than 25 K.

1 Introduction

MSP are small nanometer-sized dust particles (Hunten et al., 1980; Plane, 2012) that can change the D-region charge balance because they influence the chemical processes through charging of MSP by electrons and ions [cf. Baumann et al. (2015)]. By changing the charge balance, MSP can influence artificial heating.

https://doi.org/10.5194/angeo-2021-39
Preprint. Discussion started: 20 July 2021


Annales Geophysicae Discussions

The overall charge balance in the D-region is complex with positive ions, negative ions and cluster ions (Verronen et al., 2016). The MSP form as a result of meteor ablation that deposits the meteoric material in the higher atmosphere, which condense to MSP of sizes up to a few nanometers (Plane, 2004). Measurements on-board rockets have detected both negatively and positively charged MSPs, indicating that MSP can influence plasma densities in the D-region through charging of MSP by electrons and ions (Friedrich et al., 2012). Charging of MSP influences the charge balance mainly through electron attachment to MSP, which can results in height regions with reduced electron density, so-called electron bite-outs. Electron bite-outs change the height profile of the electron density, since the reduction in electron density occurs in altitude regions where the MSP are most abundant. Electron bite-outs within the height profile of the electron density can affect the electron temperature during artificial heating, as shown by Kassa et al. (2005).

The presence of MSP in the D-region facilitates the formation of ice particles. These ice particles contribute to the formation of strong radar echoes, called Polar Mesospheric Summer Echoes (PMSE) (Rapp and Lübken, 2004; La Hoz et al., 2006). A heater transmit powerful high-frequency radio waves into the ionosphere during artificial heating experiments. Artificial heating can induces difference phenomena in the ionosphere. Ion upwelling (Kosch et al., 2010) and artificial optical emission (Kosch et al., 2000; Kosh et al., 2014) are observed in the ionospheric F-region. Observations show that the back-scattered power of PMSE can be modified during artificial heating experiments [cf. Chilson et al. (2000); Havnes et al. (2004); Biebricher and Havnes (2012)] where the electron temperature in the ionosphere is increased artificially. In the collisional plasma of the ionospheric D-region electrons absorb the radio wave energy transmitted from the heater and heat up, increasing the electron temperature. As a consequence the intensity of the radio wave reduces (Rietveld et al., 1986; Belova et al., 1995; Kero et al., 2000, 2008).

The aim of our study is to numerically model the electron temperature during artificial heating and include the height variation of electron bite-outs by using an ionospheric model (Baumann et al., 2013) with MSP. As a comparison, we also model without MSP. The one-dimensional height-dependent ionospheric model is for quiet ionospheric conditions and includes MSP and photochemistry such as photoionization and photodetachment. We calculate the artificial heating with different radio wave frequencies and higher or lower radio wave power to investigate if this influence the electron temperature and to check the robustness of our results. We will compare night and day conditions to see if a higher electron density during daytime influence the modelled electron temperature.

This paper is organized as follows. In part 2 we present a detailed theoretical background and numerically modelling of artificial heating in the D-region. Part 3 gives a brief description of the ionospheric model. In part 4 we introduce the results. Part 5 present the discussion.

2 Artificial heating in the D-region

Powerful high frequency radio wave can heat up electrons in the ionospheric D-region by artificial heating experiments. The higher temperature of the electrons can lead to various phenomena in the whole ionosphere (e.g. Robinson (1989) and references therein). Artificial heating increases the electron temperature by transferring the radio wave energy into thermal energy

https://doi.org/10.5194/angeo-2021-39
Preprint. Discussion started: 20 July 2021

Annales Geophysicae Discussions

of electrons (Rietveld et al., 1986; Kero et al., 2007, 2008). Modelling of artificial heating in D-region altitudes show an increase in electron temperature of a factor of 10 (Belova et al., 1995; Kero et al., 2000). The EISCAT high power high frequency heating facility located in Tromsø, Norway transmit powerful high-frequency radio waves into the ionosphere during artificial heating experiments. The ESICAT radar, also located in Tromsø, Norway, can observe the ionosphere during these heating experiments. The EISCAT heating facility in Tromsø has three different antenna arrays consisting of crossed full-wave dipoles with a frequency range of 3.85-8 MHz. There are 12 transmitters that can adjust the power output from 200 MW to MW 1200, depending on the used radio frequency. The dipoles can transmit ordinary (O) circular polarization mode or extraordinary (X) circular polarization mode (Rietveld et al., 2016). The following model of the heated ionosphere, described in the next section, uses these experimental parameters of the EISCAT heating facility (Rietveld et al., 1993).

2.1 Description of model

This section describes the physical background of the electron heating process. For the implementation of these processes we rely on earlier work done by Rietveld et al. (1986); Belova et al. (1995); Kero et al. (2000); Kassa et al. (2005); Kero et al. (2007). Note that the model described in this section only cover the lower ionosphere. The heater transmits a powerful high frequency radio wave that propagates through the cold, magnetized, collisional plasma of the ionospheric D-region. The intensity *I*, or energy of the radio wave varies with height *h* according to:

$$\frac{dI}{dh} = -2kI \tag{1}$$

where *k* is the absorption coefficient, given as:

$$k = -\frac{\omega Im(n)}{c} \tag{2}$$

In Eq. 2, ω is the angular frequency of the heating radio wave, Im(n) is the imaginary part of the refractive index *n* and *c* is the speed of light. When integrated, Eq. 1 in combination with Eq. 2, yields the following expression for the intensity:

$$I(h) = \frac{ERP}{4\pi h^2} \exp\left(\frac{2\omega}{c} \int_0^h Im(n) dh\right) \tag{3}$$

where ERP is the effective radiated power. For solving Eq. 3 we need an expression for the refractive index *n*. We can derive the refractive index by using the Appleton-Hartree dispersion relation, which describes the radio waves propagation in a cold magnetized plasma and which can be applied to the ionospheric D-region. It describes the refractive index as:

$$n^2 = 1 - \frac{X}{1 - iZ - \frac{(Y\sin\theta)^2}{2(1-X-iZ)} \pm \sqrt{\frac{(Y\sin\theta)^4}{4(1-X-iZ)^2} + (Y\cos\theta)^2}} \tag{4}$$

https://doi.org/10.5194/angeo-2021-39
Preprint. Discussion started: 20 July 2021

Annales Geophysicae Discussions
Open Access
EGU

where θ is the angle between the wave vector and the direction of the magnetic field. Here, $(+)$ and $(-)$ represents the ordinary and extraordinary polarization modes, respectively. Note that the refractive index is complex $n = n_1 + in_2$. If the imaginary part is less than zero, the wave is damped. The wave damping is caused by wave energy loss through absorption by the plasma while the wave propagates through the ionosphere. Due to its lower mass, electrons absorb the energy and are thus heated, while ions and neutrals remain unheated in comparison. The dimensionless *X*, *Y* and *Z* are normalized frequencies, defined as:

$$X = \frac{\omega_{pe}^2}{\omega^2} = \frac{N_e e^2}{\varepsilon_0 m_e \omega^2} \tag{5}$$

$$Y = \frac{\omega_{ge}}{\omega} = \frac{eB}{m_e}\omega \tag{6}$$

$$Z = \frac{\nu_{en}}{\omega} \tag{7}$$

where N_e is electron density,*e* is unit charge, ε_0 is the permittivity of vacuum, m_e is electron mass, *B* is the Earth's magnetic field and ν_{en} is the electron-neutral collision frequency. How the electron-neutral collision frequency from Eq. 7 depends on electron temperature is taken from Dalgarno et al. (1967):

$$\nu_{en} = 1.7 \times 10^{-11}[N_2]T_e + 3.8 \times 10^{-10}[O_2]\sqrt{T_e} + 1.4 \times 10^{-10}[O]\sqrt{T_e} \tag{8}$$

where $[N_2]$ is the number density of molecular nitrogen, $[O_2]$ is the number density of molecular oxygen, $[O]$ is the number density of atomic oxygen and T_e is the electron temperature. Neutral densities are in units of cm^{-3} and temperature in K. Through ν_{en} the refractive index depends on the electron temperature. The electron-neutral collision frequency is high in the D-region due to the relatively low electron density in comparison to the neutral density. Therefore, electron Omic heating is the dominant D-region ionospheric response to heating. In Omic heating, electrons oscillating parallel to the radio wave electric field collides with neutrals. This causes a phase shift between the direction of the radio wave electric field and the direction of electron oscillation. Overall, electrons are scattered in a random direction. This random motion of electrons leads to absorption of wave energy, where the wave energy is transferred into thermal energy of electrons, increasing the electron temperature. To find the increased electron temperature we use the electron energy balance equation, which describes local electron energy conservation. Solving the electron energy equation gives us the electron temperature time variation due to energy input from the heater and cooling through collisions with neutrals. We have neglected thermal conductivity due to high neutral density in the D-region and neglected plasma transport. The electron energy equation is then given as:

$$\frac{dT_e}{dt} = \frac{2}{3k_b N_e}\left(Q(T_e) - L(T_e)\right) \tag{9}$$

https://doi.org/10.5194/angeo-2021-39
Preprint. Discussion started: 20 July 2021


Annales Geophysicae Discussions Open Access EGU

where k_b is Boltzmann's constant. Equation 9 is non-linear differential equation. Here $Q(T_e)$ is the power absorbed by electrons per volume:

$$Q(T_e) = 2k(T_e)I(h) = \frac{2\omega}{c} Im(n)I(h) \tag{10}$$

The electrons loose energy, and are thus cooled, through elastic and inelastic collisions with neutral species, where the inelastic collisions can excite vibrational and rotational states. The sum of all energy losses is given by the energy loss function $L(T_e)$; these are the electron cooling rates. Our cooling rates include vibrational and rotational excitation of molecular oxygen (Pavlov, 1998b) and of molecular nitrogen (Pavlov, 1998a), excitation of fine structure levels of atomic oxygen (Pavlov and Berringston, 1999) and elastic collisions between electrons and neutral species (Schunk and Nagy, 1978). Due to the low electron density in the D-region, we neglect electron-ion collision. More detailed descriptions of the electron cooling rates are in the appendix. When the heater is switched on, the electron temperature increases from its initial temperature, which is equal to the neutral temperature in the D-region, to a higher heated electron temperature. The heating time for this temperature increase is less than 100 ms due to the high collisions frequency ν_{en} in the D-region. After less than 100 ms the electron temperature has reached thermal equilibrium where $dT_e/dt = 0$. In cases where the heating modulation time is much longer than the heating time for the electron temperature, we can simplify Eq. 9 to:

$$Q(T_e) - L(T_e) = 0 \tag{11}$$

2.1.1 Implementation of model

To compute the electron temperatures during heating we numerically solve Eq. 11. At the first height the intensity is $I_0 = ERP/4\pi h^2$, the undamped radio wave. We then compute $Q(T_e)$ from Eq. 10 by using the intensity I_0, where $Q(T_e)$ is a function of T_e. We use the intensity I_0 to solve $Q(T_e) - L(T_e) = 0$ for the electron temperature by using an algorithm that combines the inverse quadratic interpolation method, bisection method and secant method (Brent, 1973; Forsythe et al., 1977). By solving $Q(T_e) - L(T_e) = 0$ we find the zero-point of Eq. 11, which gives us a new electron temperature. This new, modified electron temperature changes the refractive index since the electron-neutral collision frequency depends on electron temperature. With the changed refractive index, we recalculate the intensity, taking into account the loss due to absorption. We compute the intensity numerically by approximating the integral in Eq. 3 as a sum:

$$I(h) = \frac{ERP}{4\pi h^2} \exp\left(\frac{2\omega}{c} \sum_{h'=60km}^{h'=h} Im(n(h'))\Delta h\right) \tag{12}$$

where the first part $ERP/4\pi h^2$ represents the undamped radio wave and the part in the exponential function represents the damping effect due to absorption. The distance between each height is $\Delta h = (h') - (h'-1)$. For our case $\Delta h = 1\ \mathrm{km}$ and Δh is constant for all altitudes. In the next iteration, the intensity has changed, so there is a new zero-point for $Q(T_e) - L(T_e) = 0$,

https://doi.org/10.5194/angeo-2021-39
Preprint. Discussion started: 20 July 2021

Annales Geophysicae Discussions

Table 1. The frequencies and effective radiated power (ERP).

Case 1	Case 2	Case 3	Case 4
4 MHz	5.5 MHz	5.5 MHz	7.5 MHz
200 MW	300 MW	600 MW	1200 MW

which we compute. In Fig. 1 we show Q - L as a function of T_e with I_0, where the zero-point is illustrated as a blue-coloured star. Also in Fig. 1 we show the changed intensity, illustrated as I_1 and the zero-point for Q - L with I_1 is marked as a magenta-coloured star. We see in Fig. 1 that the zero-point of Q - L is different for I_0 and I_1. This process with a new, modified electron temperature, which changes the intensity, is repeated in an iteration scheme. The neutral temperature is the starting point in the iteration scheme. The iteration scheme is repeated until the change in the electron temperature is very small, i.e. when T_e converges. This equation visualizes the iteration for the intensity:

$$I(h+1) = I_0 - dI(h) - dI(h+1) \tag{13}$$

where $I_0 = ERP$. Here *dI(h)* represents absorption at heights below us and *dI(h+1)* represents absorption at the current height. Before we move to the next height, we sum all the absorption, so that for the next height we take into account all absorption below. In the next height, we repeat the procedure described for the first height and calculate the heated electron temperature and the new intensity. This is done for all heights, moving upward from the initial height to the final height. Our altitude range is 60-120 km. The ionospheric D-region varies in altitude range from about 50 km to 100 km, however, we model up to 120 km to see if the electron temperature at altitudes above 100 km is influenced by the presence of MSP at lower altitudes below.

We model the height-dependent heated electron temperature with initial height profiles for the following parameters: Earth's magnetic field, electron density, neutral temperature, neutral densities of molecular nitrogen, molecular oxygen and atomic oxygen. For Earth's magnetic field, we use a dipole approximation (Brekke, 2013) . The magnetic field goes into Eq. 6, which we use to compute the refractive index in Eq. 4. We compare day and night conditions to see if a higher ionization level, as during day condition, have an influence on the heated electron temperature. The used electron density height profiles during day and night conditions comes from an ionospheric model by Baumann et al. (2013). The neutral temperature and neutral densities are from MSISE-90 model (Hedin, 1991; Picone et al., 2002) with the same date, time and location as used for the ionospheric model. The parameters for the EISCAT heating radio wave include polarization, radio wave frequency and effective radiated power (ERP). The model calculations are done with X-mode transmission polarization. For the radio wave frequency and ERP, we assume a number of different typical values to see if this influence the heated electron temperature with MSP and without MSP. We ran the model for four different cases, see Table 1 (Erik Vaberg, personal communication). Figure 2 shows a schematic on how we computed the heated electron temperature by combining artificial heating and the electron density from the ionospheric model. In the next section we briefly describe the ionospheric model.

https://doi.org/10.5194/angeo-2021-39
Preprint. Discussion started: 20 July 2021

Annales Geophysicae Discussions
Open Access
EGU

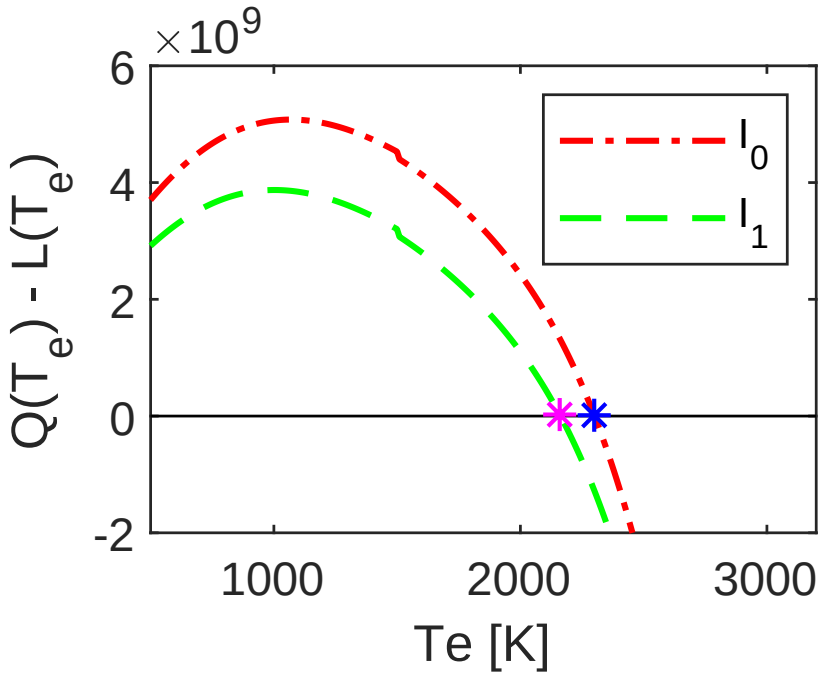

Figure 1. Illustration of $Q(T_e) - L(T_e)$ as a function of electron temperature with intensity I_0 (the undamped radio wave) and I_1 (radio wave with damping). Here $I_0 > I_1$. The units of $Q(T_e) - L(T_e)$ is energy per volume per second $\mathrm{eVm^{-3}s^{-1}}$. With a different intensity, we change the location of the zero-point, where $Q(T_e) - L(T_e) = 0$. The zero-point is marked as a blue star for I_0 or a magenta star for I_1.

3 Background ionospheric model

Here in this part we give a brief description of a one-dimensional height-dependent ionospheric model for the D-region, which includes MSP, developed by Baumann et al. (2013). For the full description, see Baumann et al. (2013) and references therein. The one-dimensional height-dependent ionospheric model is run for quiet ionospheric conditions between heights of 60-120 km and includes electron, positively and negatively charged ions, neutral MSP, singly positively and singly negatively charged MSP. Multiply charged dust is unlikely to occur since the MSP are very small. Initial conditions for the height and size-dependent MSP number density profile come from Megner et al. (2006), where the size range is from 0.2 nm to 41 nm. Above 100 km, the density of MSP is assumed to be very small. The computation scheme includes chemical reactions like the standard plasma reactions for electrons and ions, plasma capture reactions by MSP and photo reactions such as photo ionization and photo detachment of MSP. The standard plasma reactions includes ionization, dissociative recombination, electron attachment to neutrals, electron detachment from negative ions and ion-ion recombination. Figure 3 shows a schematic of the underlying ionospheric model. By solving the time-dependent rate equations for the six species, the ionospheric model computes number densities of electrons, ions and MSP. The rate equations describes how the concentration of a given species varies with time by looking at the local production rate and local loss rate. The modelling is done with and without the MSP, as a comparison. For

https://doi.org/10.5194/angeo-2021-39
Preprint. Discussion started: 20 July 2021

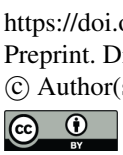

Annales Geophysicae Discussions
Open Access
EGU

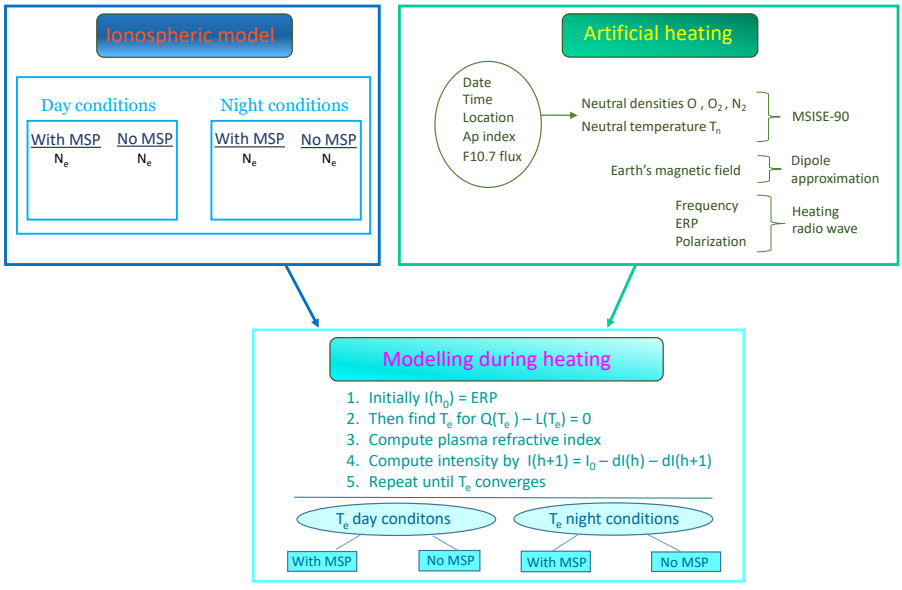

Figure 2. Schematic showing how we combined artificial heating and the electron density from the ionospheric model in order to compute the heated electron temperature. The parameters for artificial heating include frequency, effective radiated power (ERP) and polarization of the heating radio wave, Earth's magnetic field and neutral densities and neutral temperature.

the initial conditions, the following come from the SIC model: Number densities of electrons, positive ions and negative ions, the temperature of ions and electrons, the reaction rate coefficients for the standard plasma reactions and average ion mass. The SIC model was run for 8. September 2010, Andenes, Norway, 69° North and 16° East at 23:55 LT (night conditions) and 12:15 LT (day conditions).

4 Results

4.1 Night conditions

This section present results for the electron temperature modelled during artificial heating with and without the presence of MSP for night condition. The main results are that from 80 km and above the heated electron temperature is higher when MSP are present, and this applies to all cases with different frequencies and ERP. In Fig. 4 we show results for electron density influenced by MSP. As a comparison, we ran the model without the influence of MSP. We see in Fig. 4 that there is a reduction in electron density, an electron bite-out, due to the presence of MSP, predominantly between heights 80-100 km. There is an electron bite-out between 70-80 km, but it is significantly smaller than between 80-100 km. Between 100-120 km, the electron bite-outs are not present. We see that electron bite-outs changes the height profile of the electron density.

Figure 5 presents results for the heated electron temperature for case 1-4. The heated electron temperature is computed with the electron density from Fig. 4. In Fig. 5 we see that the electron temperature is higher for altitudes above 80 km when MSP

https://doi.org/10.5194/angeo-2021-39
Preprint. Discussion started: 20 July 2021

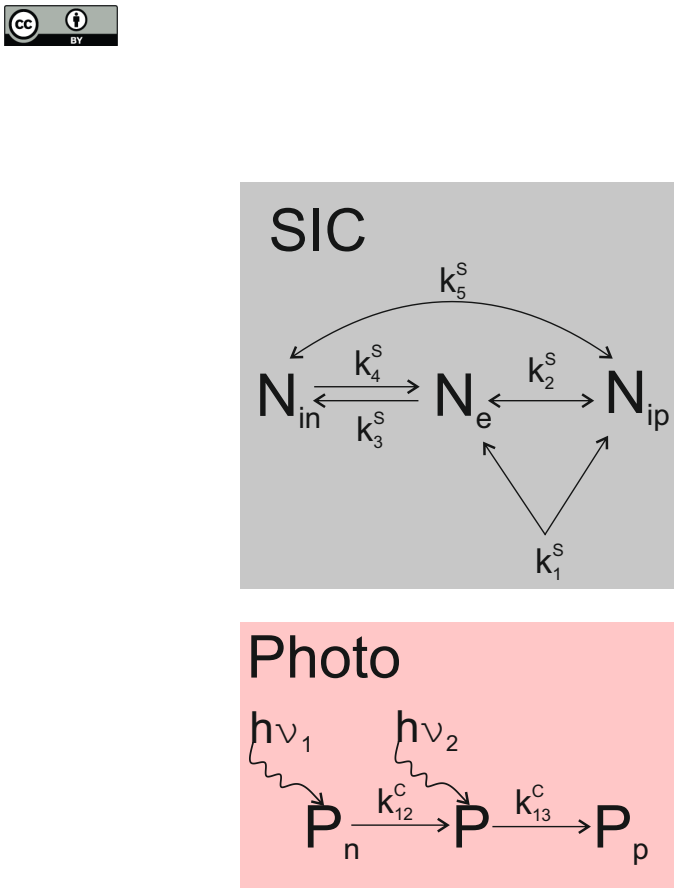

Figure 3. Schematic of the underlying ionospheric model. Grey shaded reactions are SIC reactions rates generalized to the reduced set of ionospheric constituents (N_{in}- negative ions, N_e- electrons, N_{ip}- positive ions), green shaded are charge carrier capture processes by MSP (P_n- negative MSP, P- neutral MSP, P_p- positive MSP) and red shaded are the photo detachment and photo ionization of MSP. The $k_1 - k_{13}$ are reaction rates coefficients. For details on the individual reactions see Baumann et al. (2013)

are present. The shape of the height profile varies as well, where the heated electron temperature decreases more slowly when MSP are present so that the shape of the height profile is more flat. Without MSP, the electron temperature decreases faster and it has a different overall shape. Below 80 km, the heated electron temperature is the same with and without MSP. A comparison of the four different cases show similar results for the heated electron temperature in Fig. 5. The electron temperature is higher when MSP are present for all five different cases and the shape is also similar. In addition, for all five cases the heated electron temperature with and without MSP are the same up to 80 km. We also see that a higher ERP results in a higher electron temperature, where T_e reaches almost 3000 K for case 4 with ERP 1200 MW.

Figure 6 shows the absolute difference between the heated electron temperature modelled with and without MSP, i.e. how much higher the heated electron temperature is with MSP compared to without MSP. The difference in T_e increases from 80 km and reaches a maximum between 90-100 km. From 100 km and on, the difference in T_e starts to decrease. The difference in T_e increases for higher ERP. For case 4 with a frequency of 7.5 MHZ and ERP 1200 MW, the difference in T_e at around 100 km is almost 1000 K, while for case 3 with a frequency of 5.5 MHZ and ERP 600 MW the difference in T_e at around 95

https://doi.org/10.5194/angeo-2021-39
Preprint. Discussion started: 20 July 2021

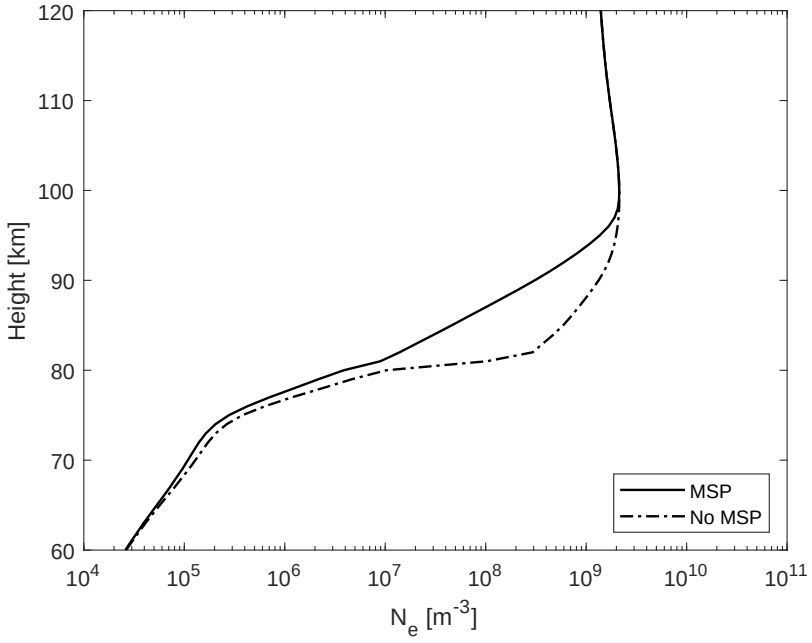

Figure 4. Electron density during night conditions, where the electron density come from the ionospheric model. The legend show model run with and without the MSP.

km is 700 K. For the lower ERP of 200 MW with frequency 4 MHZ (case 1) or ERP of 300 MW with frequencies 5.5 MHZ (case 2), the difference in T_e is between 200-500 K at 95 km.

In Fig. 5 a small feature appears in some of the plots when the electron temperature is around 1500 K. The location of the feature appears at different altitudes, varying between 80-110 km. Out of the four different cases that we considered for comparison (4 cases with MSP and 4 cases without MSP, so 8 all together), the feature appears in 4 out of 8 plots, 1 with MSP and 3 without MSP.

4.1.1 Day conditions

This section presents results for electron temperature modelled during artificial heating with and without the presence of MSP for day condition. Figure 7 shows electron density with and without MSP. As for night conditions the electron density come from the ionospheric model. We see that the electron bite-outs are not present in Fig. 7. Figure 8 shows the heated electron temperature for case 1-4. We see that the heated electron temperature is the same with and without MSP. We find that the absolute difference between the electron temperature modelled with and without MSP is less than 25 K for all cases 1-4. Compared to night conditions, the day conditions electron temperature is lower. For case 1-3 during day conditions, the electron temperature is below 2000 K for all altitudes. At around 90 km, the electron temperature is back to the neutral temperature for all cases 1-4.

https://doi.org/10.5194/angeo-2021-39
Preprint. Discussion started: 20 July 2021

Annales Geophysicae Discussions
Open Access
EGU

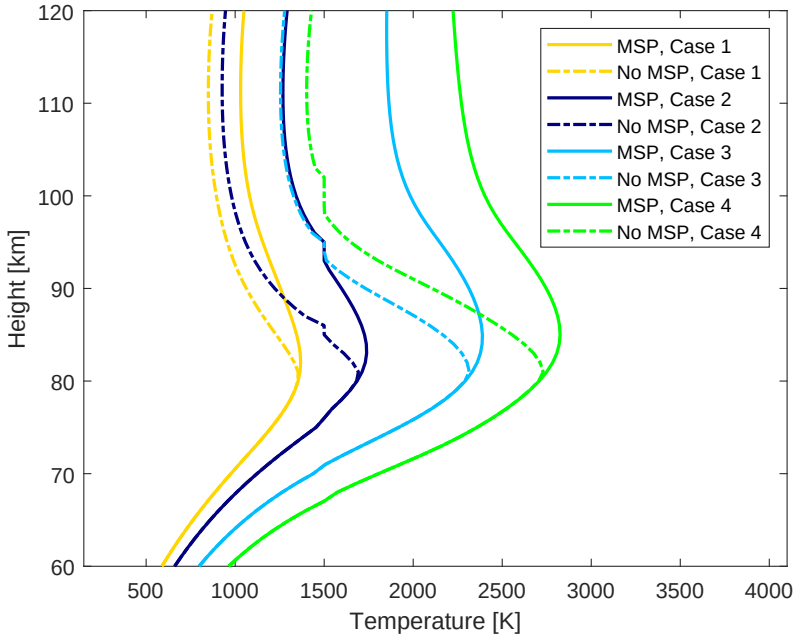

Figure 5. Night condition results for modelled electron temperature during heating as a function of height for case 1-4. The legend show model run with and without the MSP and for the different cases 1-4.

5 Discussion

Both Kero et al. (2007) and Senior et al. (2010) found that current theoretical models most likely overestimate artificial heating in the D-region compared to observations of the heating effect in the D-region. Why the theoretical models overestimates artificial heating in the D-region remains an open question. Kero et al. (2007) studied how artificial heating influences cosmic radio noise absorption and found that the observed enhancement of cosmic radio noise absorption during heating is lower than predicted theoretically. Senior et al. (2010) used a cross-modulation technique with the EISCAT radar and found that the model overestimates the diagnostic wave absorption. In the study by Senior et al. (2010), the authors note that electron bite-outs located at PMSE layer altitudes might influence the model, but that the influence is probably small, because the bite-outs are located too high in altitude. They investigate the influence of the electron bite-outs by scaling the whole electron density profile with a factor of 2 or 0.5. However, they do not include the height variation of the electron density profile when electron bite-out are present. We find that electron bite-outs are only present at certain altitudes. The magnitude of the electron bite-outs varies within these altitude, for instance, the electron bite-out is significantly larger between 80-100 km compared to between 70-80 km. In our study, we have modelled the electron temperature during heating and included the height variation of the electron bite-outs. We have included the height variation of electron bite-outs by using the ionospheric model with MSP, which presents a simplified model of the D-region by including height and size-dependent MSP distribution in a reaction scheme with

https://doi.org/10.5194/angeo-2021-39
Preprint. Discussion started: 20 July 2021

Annales Geophysicae Discussions
Open Access
EGU

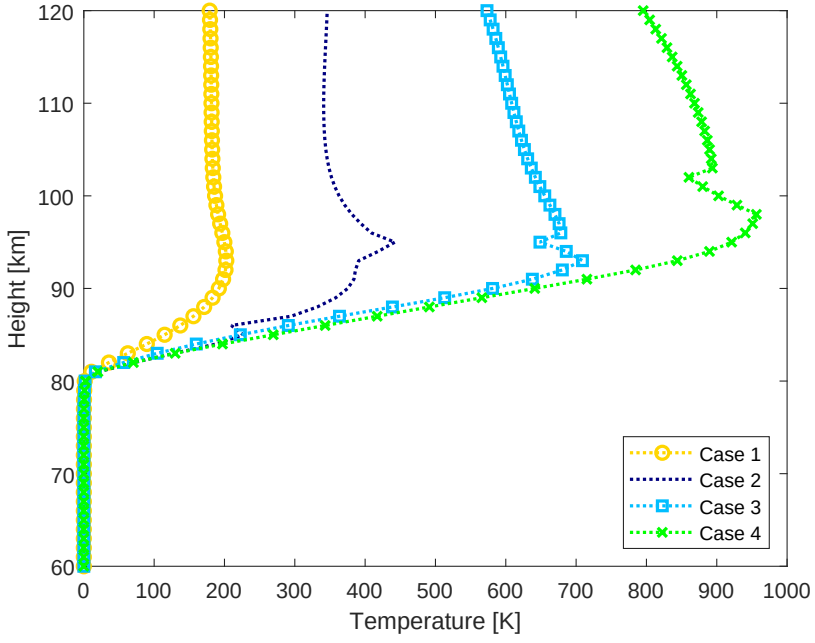

Figure 6. Absolute difference between the electron temperature modelled with and without the MSP during night conditions. The legend show model run for the different cases 1-4.

electrons, ions and neutral and charged MSP. This enables us to have a more realistic representation of the height variation of the electron bite-outs. In a future study we will make a detailed comparison of our results to observations of the electron temperature during heating. This detailed comparison can investigate if the presence of MSP can explain the discrepancy between model and observations.

Figure 5 for night conditions show that the electron temperature is higher and decreases more slowly when MSP are present. An explanation for why the heated electron temperature decreases more slowly is that with electron bite-outs at certain altitudes, the heating above these heights will be increased since less of the wave energy is absorbed within the electron bite-outs. The absorption of wave energy depend on electron density and the absorption decreases with decreasing electron density. We see this effect in Fig. 9, which shows absorbed radio wave energy as a function of height. Here, less wave energy is absorbed when MSP are present. More wave energy is absorbed at higher altitudes, slightly above where the electron bite-outs are largest in magnitude. The cooling rates also depend on electron density and decreases at higher altitudes due to a lower electron-neutral collision frequency since the neutral density is lower. The electron cooling - heating equality is reached at higher electron temperatures as more wave energy remains in the MSP case compared to the case without MSP. An electron bite-out at lower altitudes can lead to an increased electron temperature at higher altitudes above.

The results of our study shows that the frequency of the transmitted radio wave only plays a minor role, lower frequency only slightly shifts the start of the heated ionosphere to a higher altitude. We also see that the increased electron temperature

https://doi.org/10.5194/angeo-2021-39
Preprint. Discussion started: 20 July 2021

Annales Geophysicae Discussions
Open Access
EGU

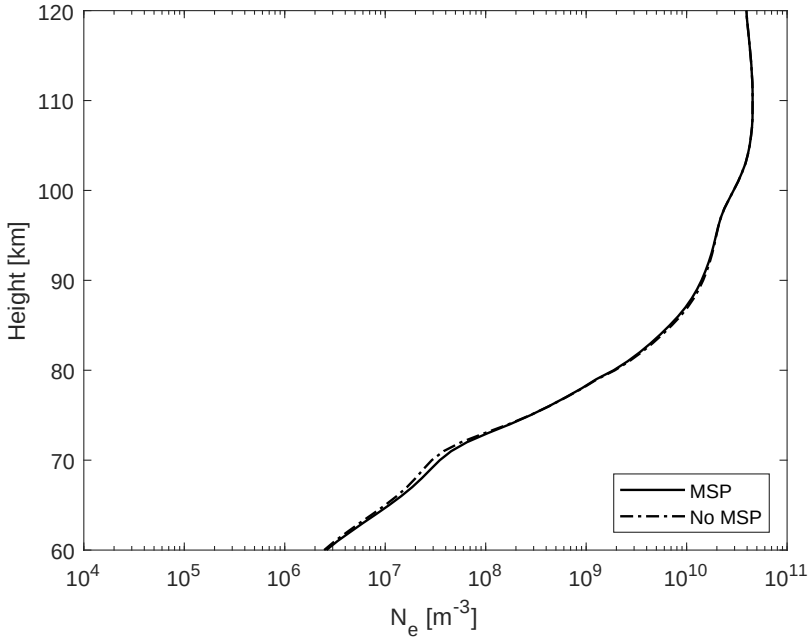

Figure 7. Day condition results for electron density, which come from the ionospheric model. The legend show model run with and without the MSP.

due to the presence of MSP extends up to 120 km in the E-region. Our model for the heated electron temperature might not be applicable for the E-region, however, this is beyond the scope of this paper. The results from this study agrees with Kassa et al. (2005), where an electron bite-out inserted as a linearly decreasing 'toy model' between 84-86 km during PMSE conditions resulted in an increased modelled electron temperature within and above the electron bite-out.

Figure 8 shows that day condition electron temperature is the same with and without MSP. This indicate that for day condition, MSP are less important for the heated electron temperature. A higher ionization level, and thus a much higher electrons density, means that loss of electrons, like electron attachment to MSP, is less important. Generally, the electron temperature is lower for day conditions. This is because the electron density is higher during the day, also at lower heights. The electron density in Fig. 7 is $2.5 \cdot 10^6$ m^{-3} at 60 km for day conditions, while for night conditions the electron density in Fig. 4 is $2.6 \cdot 10^4$ m^{-3} at 60 km. With a higher electron density as during day conditions, the radio wave energy is absorbed already at lower heights.

In Fig. 5 there is a feature in some of the plots of the heated night condition electron temperature. This feature can resembles a small second maximum, or it might just be an artefact. It appeared when we included the temperature dependence of the cooling rates for vibrational excitation of molecular nitrogen; the values from Pavlov (1998a) that we use are different for the temperatures $300 \leq T_e \leq 1500$ K and for those $T_e > 1500$ K. The feature that we note is at electron temperature around 1500 K. The feature disappears if we apply the same values for vibrational excitation of molecular nitrogen over the entire range

https://doi.org/10.5194/angeo-2021-39
Preprint. Discussion started: 20 July 2021

Annales Geophysicae Discussions
Open Access
EGU

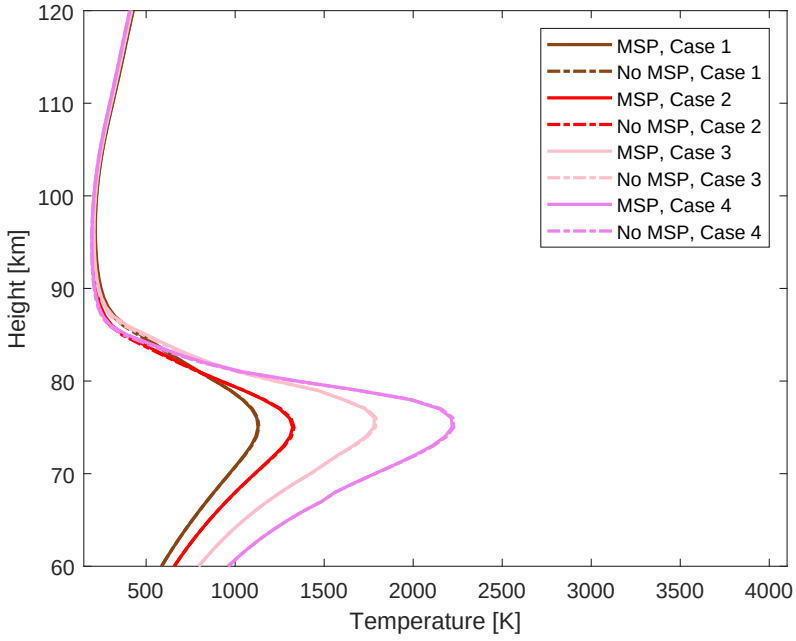

Figure 8. Day condition results for the modelled electron temperature during heating as a function of height. The legend show model run with and without the MSP and for the different cases 1-4.

of temperatures and disregard the difference for the $T_e \leq 1500$ K case. Kero et al. (2008) found a second maximimum in the EISCAT incoherent scatter observations for the heated electron temperature in the D-region, which they could not explain. The feature in Fig. 5 might be a second maximum or it might be an artefact caused by problems in the numerical modelling when switching between values for $T_e \leq 1500$ K and $T_e > 1500$ K. Whether the feature is an artefact or not is unknown at the present and can be investigated further. The feature is not seen in the day condition electron temperature in Fig. 8.

6 Conclusions

The presented model calculations show that the presence of MSP can influence the electron temperature during artificial heating. The influence of the MSP varies with ionospheric conditions. For night conditions, the results show a higher heated electron temperature above altitudes of 80 km when MSP are present. We found differences of up to 1000 K in temperature for calculations with and without MSP. Below 80 km of altitude for night conditions the difference in temperature are small for model calculations with and without MSP. For day conditions, the difference between the heated electron temperature with MSP and without MSP is less than 25 K. Our results indicate that MSP can influence both the magnitude and shape of the heated electron temperature above 80 km, however this depends on ionospheric conditions.

https://doi.org/10.5194/angeo-2021-39
Preprint. Discussion started: 20 July 2021

Annales Geophysicae Discussions
Open Access
EGU

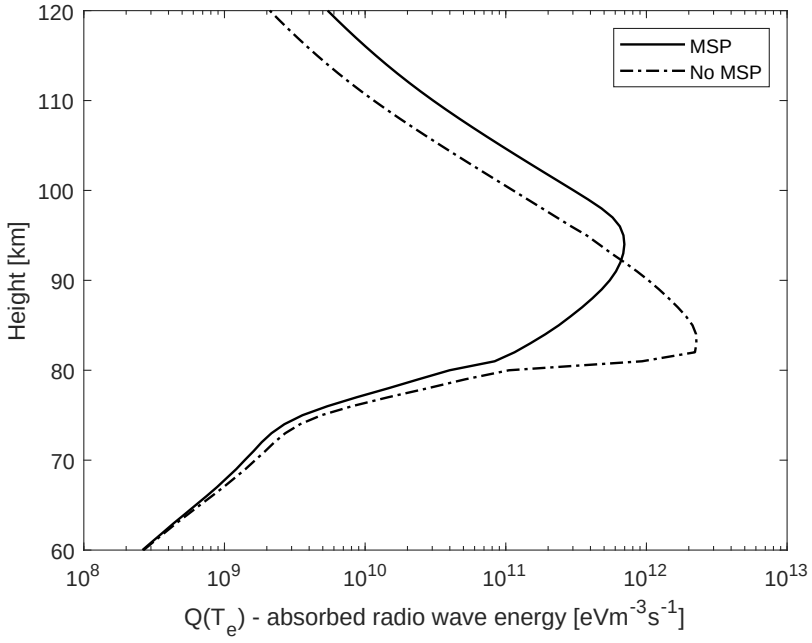

Figure 9. Absorbed radio wave energy Q $(= L_{sum})$ as a function of height for night condition and case 2 (5.5 MHz and ERP 600 MW). The legend show model run with and without the MSP. We show this figure to illustrate how the absorbed power varies with and without MSP.

Code availability. A function that computes the electron temperature and radio wave intensity during artificial heating, which includes the electron cooling rates, will be made available.

Appendix A: Electron cooling rates

The electrons loose energy through collisions with the neutral gases. The dominant cooling processes related to $[N_2]$ and $[O_2]$ are the energy transfer via vibrational and rotational excitation [cf. Rietveld et al. (1986); Gustavsson et al. (2010)]. In addition, atomic oxygen *[O]* plays an important role through the impact excitation of fine structure levels of its ground state (see Pavlov and Berringston (1999) and references given there). We here repeat the cooling rates that are used. The sum of the electron cooling rates are the energy loss function, given as:

$$L(T_e) = L_{fs}(O) + L_{vib}(N_2) + L_{rot}(N_2) + L_{vib}(O_2) + L_{rot}(O_2) + L_{el}(N_2) + L_{el}(O_2) + L_{el}(O) \quad \text{(A1)}$$

The unit of $L(T_e)$ are in $\mathrm{Jm^{-3}s^{-1}}$.

https://doi.org/10.5194/angeo-2021-39
Preprint. Discussion started: 20 July 2021

Annales Geophysicae Discussions
Open Access
EGU

To describe the excitation of fine structure levels of atomic oxygen, we use Eq. 15 from Pavlov and Berringston (1999):

$$\begin{aligned} L_{fs}(O) = N_e[O]D^{-1}(S_{10}\{1-\exp[98.9(T_e^{-1}-T_n^{-1})]\} \\ +S_{20}\{1-\exp[326.6(T_e^{-1}-T_n^{-1})]\} \\ +S_{21}\{1-\exp[227.7(T_e^{-1}-T_n^{-1})]\}) \end{aligned} \tag{A2}$$

The units of equation A2 is $\mathrm{eVcm^{-3}s^{-1}}$ and T_n is the neutral temperature. Both T_e and T_n are in K. The equation is based on assuming that the electron velocity distribution is Maxwellian. The terms *D*, S_{21}, S_{20} and S_{10} are:

$$D = 5 + \exp(-326.6 \cdot T_n^{-1}) + 3\exp(-227.7 \cdot T_n^{-1}) \tag{A3}$$

$$S_{21} = (1.863 \cdot 10^{-11}) \tag{A4}$$

$$S_{20} = (1.191 \cdot 10^{-11}) \tag{A5}$$

$$S_{10} = (8.249 \cdot 10^{-16} \cdot T_e^{0.6} \exp(-227.7 \cdot T_n^{-1}) \tag{A6}$$

The S_{ij} denote the transitions between the three fine structure levels of the atomic oxygen ground state.

For vibrational excitation of molecular nitrogen, we use Eq. 11 from Pavlov (1998a) for a Boltzmann distribution:

$$\begin{aligned} L_{vib}(N_2) = N_e[N_2]\{1-\exp(-E_1/T_{vib})\} \\ \times\sum_{v=1}^{10} Q_{0v}\{1-\exp[vE_1(T_e^{-1}-T_{vib}^{-1})]\} \\ +N_e[N_2]\{1-\exp(-E_1/T_{vib})\}(\exp(-E_1/T_{vib})) \\ \times\sum_{v=2}^{9} Q_{1v}\{1-\exp[(v-1)E_1(T_e^{-1}-T_{vib}^{-1})]\} \end{aligned} \tag{A7}$$

where $E_1 = 3353$ K is the energy of first vibrational level of $[N_2]$ and we assume that the vibrational temperature is equal to the neutral temperature. The units of $L_{vib}(N_2)$ is $\mathrm{eVcm^{-3}s^{-1}}$. Here, Q_{0v} describes excitation transitions from ground states and Q_{1v} describes excitation transitions from the first vibrational state. For Q_{0v} and Q_{1v}, we implement Eq. 19 and Eq. 20 from Pavlov (1998a), respectively:

$$\log Q_{0v} = A_{0v} + B_{0v}T_e + C_{0v}Te^2 + D_{0v}Te^3 + F_{0v}Te^4 - 16 \tag{A8}$$

https://doi.org/10.5194/angeo-2021-39
Preprint. Discussion started: 20 July 2021

Annales Geophysicae Discussions
Open Access
EGU

$$\log Q_{1v} = A_{1v} + B_{1v}T_e + C_{1v}Te^2 + D_{1v}Te^3 + F_{1v}Te^4 - 16 \tag{A9}$$

where the coefficients $A_{0v}, B_{0v}, C_{0v}, D_{0v}, F_{0v}$ to compute Q_{0v} and $A_{1v}, B_{1v}, C_{1v}, D_{1v}, F_{1v}$ to compute Q_{1v} come from tables in Pavlov (1998a). For Q_{0v} from Table 1 for $300 \leq T_e \leq 1500$ K and from Table 2 for $T_e > 1500$ K. For Q_{1v} from Table 3 for $1500 \leq T_e \leq 6000$ K. However, there is no table for Q_{1v} for $T_e < 1500$ K. Both Q_{0v} and Q_{1v} have units $\mathrm{eVcm^3s^{-1}}$. Rotational excitation of molecular nitrogen come from Eq. A2 in Pavlov (1998a):

$$C = 3.51 \cdot 10^{-14} \tag{A10}$$

$$L_{rot}(N_2) = C[N_2]N_e(T_e - T_n)Te^{-0.5} \tag{A11}$$

The units of C and $L_{rot}(N_2)$ are $\mathrm{eVcm^3s^{-1}K^{-0.5}}$ and $\mathrm{eVcm^{-3}s^{-1}}$, respectively.

For vibrational excitation of molecular oxygen we use Eq. 8 from Pavlov (1998b), which assume a Boltzmann distribution:

$$L_{vib}(O_2) = N_e[O_2]\sum_{v=2}^{7} Q^*_{0v}\{1 - \exp[vE_1(T_e^{-1} - T_{vib}^{-1})]\} \tag{A12}$$

in units $\mathrm{eVcm^{-3}s^{-1}}$ and where $E_1 = 2239$ K is the energy of the first vibrational level of $[O_2]$ and we set $T_{vib} = T_n$. Here Q_{0v} describes excitation transitions from ground states. Q_{0v} come from Eq. 11 in Pavlov (1998b):

$$Q^*_{0v} = A_v \exp\{(1 - B_v Te^{-1})(C_v + D_v \sin[F_v(T_e - G_v)])\} \tag{A13}$$

where the coefficients $A_v, B_v, C_v, D_v, F_v, G_v$ as a function of vibrational level come from Table 1 of Pavlov (1998b). For rotational excitation of $[O_2]$ we use Eq. 16, also from Pavlov (1998b):

$$C_{O_2} = 5.2 \cdot 10^{-15} \tag{A14}$$

$$L_{rot}(O_2) = C_{O_2}[O_2]N_e(T_e - T_n)T_e^{-0.5} \tag{A15}$$

where C_{O_2} have units $\mathrm{eVcm^3s^{-1}K^{-0.5}}$ and $L_{rot}(O_2)$ has units $\mathrm{eVcm^{-3}s^{-1}}$. For elastic collisions between electrons and neutrals (molecular nitrogen, molecular oxygen and atomic oxygen, respectively) we implement Eq. 43a, 43b, 43c from Schunk and Nagy (1978):

$$L_{el}(N_2) = N_e[N_2]1.77 \cdot 10^{-19}T_e(T_e - T_n)(1 - 1.21 \cdot 10^{-4}T_e) \tag{A16}$$

https://doi.org/10.5194/angeo-2021-39
Preprint. Discussion started: 20 July 2021

Annales Geophysicae Discussions
Open Access
EGU

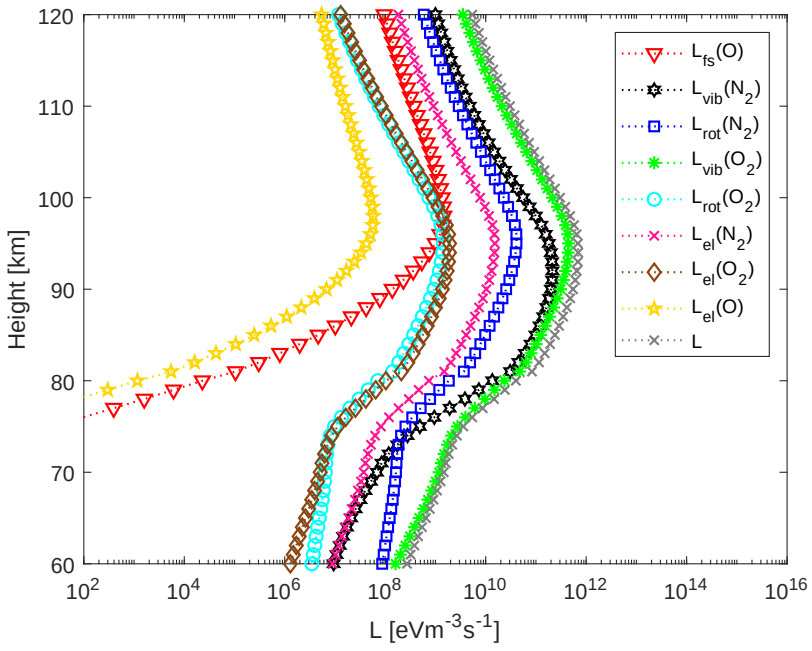

Figure A1. Night condition electron cooling rates with MSP as a function of height for a heated electron temperature. The frequency is 5.5 MHz and ERP is 600 MW. The legend show the different cooling rates as described in this section.

330

$$L_{el}(O_2) = N_e[O_2]1.21 \cdot 10^{-18}\sqrt{T}_e(T_e - T_n)(1 + 3.6 \cdot 10^{-2}\sqrt{T}_e) \tag{A17}$$

$$L_{el}(O) = N_e[O]7.9 \cdot 10^{-19}\sqrt{T}_e(T_e - T_n)(1 + 5.7 \cdot 10^{-4}T_e) \tag{A18}$$

In Fig. A1 and Fig. A2 we present height profiles for electron cooling rates for night conditions. We show electron cooling
335 rates for a heated electron temperature. Figure A1 show cooling rates where MSP are present, while Fig. A2 shows cooling rates where MSP are not present. The frequency is 5.5 MHz and ERP is 600 MW.

https://doi.org/10.5194/angeo-2021-39
Preprint. Discussion started: 20 July 2021

Annales Geophysicae Discussions
Open Access
EGU

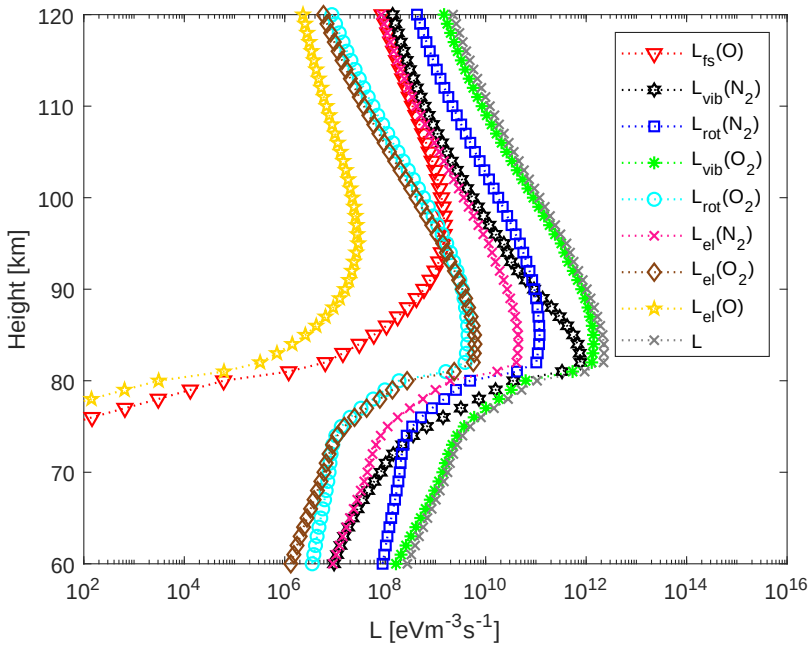

Figure A2. Night condition electron cooling rates without MSP as a function of height for a heated electron temperature. The frequency is 5.5 MHz and ERP is 600 MW. The legend show the different cooling rates as described in this section.

Author contributions. Margaretha Myrvang made the artificial heating program and prepared the initial manuscript. Carsten Baumann developed the ionospheric model. Ingrid Mann suggested the topic and supervised the project. All authors contributed to the preparation of the manuscript.

Competing interests. Ingrid Mann is editor-in-chief and topical editor of ANGEO.

Acknowledgements. We would like to thank Ove Havnes for providing us with a program from Meseret Kassa, which computes the electron temperature during heating. We have compared our results to the program from Meseret Kassa. In addition, we would like to thank Antti Kero for suggesting to look at how the presence of MSP can influence artificial heating. Lastly, we would like to thank Björn Gustavsson for helping us with the theory of artificial heating.

This work was supported by the Research Council of Norway through grant numbers: The Mesospheric Dust in Small Size Limit NFR 275503. The publication charges for this article have been funded by a grant from the publication fund of UiT, The Arctic University of Norway.

https://doi.org/10.5194/angeo-2021-39
Preprint. Discussion started: 20 July 2021

References

Baumann, C., Rapp, M., Kero, A., and Enell, C.-F.: Meteor smoke influence on the D-region charge balance –review of recent in situ measurements and one-dimensional model results, Ann. Geophys., 31, 2049–2062, https://doi.org/10.5194/angeo-31-2049-2013, 2013.

Baumann, C., Rapp, M., Anttila, M., Kero, A., and Verronen, P.: Effects of meteoric smoke particles on the D-region ion chemistry, J. Geophys. Res. Space Physics, 120, 10,823–10.839, https://doi.org/10.1002/2015JA021927, 2015.

Belova, E. G., Pashin, A. B., and Lyatsky, W. B.: Passage of a powerful HF radio wave through the lower ionosphere as a function of initial electron density profiles, Journal of Atmospheric and Terrestrial Physcis, 57, 265–272, 1995.

Biebricher, A. and Havnes, O.: Non-equilibrium modelling of the PMSE overshoot effect revisited: A comprehensive study, J. Plasma Physics, 78, 303–319, https://doi.org/10.1017/S0022377812000141, 2012.

Brekke, A.: Physics of the upper polar atmosphere, Springer-Verlag, Berlin Heidelberg, 2st edn., 2013.

Brent, R.: Algorithms for Minimization Without Derivatives, Prentice-Hall, Englewood Cliffs, New Jersey, 1973.

Chilson, P. B., Belova, E., Rietveld, M. T., Kirkwood, S., and Hoppe, U.-P.: First artificially induced modulation of PMSE using the EISCAT heating facility, Geophys. Res. Lett., 27(23), 3801–3804, https://doi.org/10.1029/2000GL011897, 2000.

Forsythe, G. E., Malcolm, M. A., and Mole, C. B.: Computer Methods for Mathematical Computations, Prentice-Hall, Englewood Cliffs, New Jersey, 1st edn., 1977.

Friedrich, M., Rapp, M., Blix, T., Hoppe, U. P., Torkar, K., Robertsen, S., Dickson, S., and Lynch, K.: Electron loss and meteoric dust in the mesosphere, Ann. Geophys., 30, 1495–1501, https://doi.org/10.5194/angeo-30-1495-2012, 2012.

Gustavsson, B., Rietveld, M. T., Ivchenko, N. V., and Kosch, M. J.: Rise and fall of electron temperature: Ohmic heating of ionospheric electrons from underdense HF radio wave pumping, Journal of geophysical research, 115, A12332, https://doi.org/10.1029/2010JA015873, 2010.

Havnes, O., Hoz, C. L., , Biebricher, A., Kassa, M., Næsheim, L. I., and Zivkovic, T.: Investigation of the mesospheric PMSE conditions by use of the new overshoot effect, Phys. Scripta, T107, 70–78, 2004.

Hedin, A. E.: Extension of the MSIS thermosphere model into the middle and lower atmosphere, J. Geophys. Res., 96, 1159–1172, 1991.

Hunten, D. M., Turco, R. P., and Toon, O. B.: Smoke and Dust Particles of Meteoric Origin in the Mesosphere and Stratosphere, J. Atmos. Sci., 37, 1342–1357, 1980.

Kassa, M., Havnes, O., and Belova, E.: The effect of electron bite-outs on artificial electron heating and the PMSE overshoot, Ann. Geophys., 23, 3633–3643, 2005.

Kero, A., Bösinger, T., Pollari, P., Turunen, E., and Rietveld, M.: First EISCAT measurements of electron-gas temperature in the artificially heated D-region ionosphere, Ann. Geophys., 18, 1210–1215, 2000.

Kero, A., Enell, C. F., Ulich, T., Turunen, E., Rietveld, M. T., and Honary, F. H.: Statistical signature of active D-region HF heating in IRIS riometer data from 1994-2004, Ann. Geophys., 25, 407–415, 2007.

Kero, A., Vierinen, J., Enell, C. F., Virtanen, I., and Turunen, E.: New incoherent scatter diagnostic methods for the heated D-region ionosphere, Ann. Geophys., 26, 2273–2279, 2008.

Kosch, M. J., Rietveld, M. T., Hagfors, T., and Leyser, T. B.: High-latitude HF-induced airglow displaced equatorwards of the pump beam, Geophys. Res. Lett, 27(17), 2817–2820, https://doi.org/10.1029/200GL003754, 2000.

Kosch, M. J., Ogawa, Y., Rietveld, M. T., Nozawa, S., and Fujii, R.: An analysis of pump-induced artificial ionospheric ion upwelling at EISCAT, J. Geophys., 115, A12317, 623–637, https://doi.org/10.1029/2010JA015854., 2010.

https://doi.org/10.5194/angeo-2021-39
Preprint. Discussion started: 20 July 2021

Kosh, M., Bryers, J. C., Rietveld, M., Yeoman, T. K., and Ogawa, Y.: Aspect angle sensitivity of pump-induced optical emission at EISCAT, Earth Planets Space, 66, 159, https://doi.org/10.1186/s40623-014-0159-x, 2014.

La Hoz, C., Havnes, O., Næsheim, L. I., and Hysell, D. L.: Observations and theories of polar mesospheric summer echoes at a Bragg wavelength of 16 cm, Geophys. Res., 111, D04203, 623–637, https://doi.org/10.1029/2005JD006044, 2006.

Megner, L., Rapp, M., and Gumbel, J.: Distribution of meteoric smoke- sensitivity to microphysical properties and atmospheric conditions, Atmos. Chem. Phys., 6, 4415–4426, https://doi.org/10.5194/acp-6-4415-2006, 2006.

Pavlov, A. V.: New electron energy transfer rates for vibrational excitation of N2, Ann. Geophys., 16, 176–182, 1998a.

Pavlov, A. V.: New electron energy transfer and cooling rates for vibrational excitation of O2, Ann. Geophys., 16, 1007–1013, 1998b.

Pavlov, A. V. and Berringston, K. A.: Cooling rates of thermal electrons by electron impact excitation of fine structure levels of atomic oxygen, Ann. Geophys., 17, 919–924, 1999.

Picone, J., Hedin, A., Drob, D., and Aikin, A.: NRLMSISE-00 empirical model of the atmosphere: Statistical comparisons and scientific issues, J. Geophys. Res., 107(A12), 1468, https://doi.org/10.1029/2002JA009430, 2002.

Plane, J. M. C.: A time-resolved model of the mesospheric Na layer: constraints on the meteor input function, Atmospheric Chemistry and Physics, European Geosciences Union, 4(3), 627–638, https://doi.org/10.5194/acp-4-627-2004, 2004.

Plane, J. M. C.: Cosmic dust in the Earth's atmosphere, Chem. Soc. Rev., 41, 6507–6518, https://doi.org/10.1039/c2cs35132c, 2012.

Rapp, M. and Lübken, F.-J.: Polar mesosphere summer echoes (PMSE): review of observations and current understanding, Atmos. Chem. Phys., 4, 2601—-2633, https://doi.org/10.5194/acp-4-2601-2004, 2004.

Rietveld, M. T., Kopka, H., and Stubbe, P.: D-region characteristics deduced from pulsed ionsospheric heating during auroral electrojet conditions, Journal of Atmospheric and Terrestrial Physcis, 48, 311–326, 1986.

Rietveld, M. T., Kohl, H., Kopka, H., and Stubbe, P.: Introduction to ionospheric heating at Tromsø. Experimental overview, J. Atmos. Terr. Phys., 55, 577–599, 1993.

Rietveld, M. T., Senior, A., Markkanen, J., and Westman, A.: New capabilities of the upgraded EISCAT high-power HF facility, Radio Sci, 51, 1533–1546, https://doi.org/10.1002/2016RS006093, 2016.

Robinson, T.: The heating of the high latitude ionossphere by high power radio waves, Physics Reports (Review Section of Physics Letters), 179, 79—-209, 1989.

Schunk, R. W. and Nagy, A. F.: Electron temperature in the F-region of the ionosphere: Theory and observations, Rev. Geophys., 16, 355–399, 1978.

Senior, A., Rietveld, M. T., Kosch, M. J., and Singer, W.: Diagnosing radio plasma heating in the polar summer mesosphere using cross modulation: Theory and observations, Journal of geophysical research, 115, A09318, https://doi.org/10.1029/2010JA015379, 2010.

Verronen, P. T., Andersson, M. E., Marsh, D. R., Kovacs, T., and Plane, J. M. C.: WACCM-D—Whole Atmosphere Community Climate Model with D-region ion chemistry, J. Adv. Model. Earth Syst., 8, 954—975, https://doi.org/10.1002/2015MS000592, 2016.